Appl. Phys. A 69, 297–304 (1999) / Digital Object Identifier (DOI) 10.1007/s003399900120

Applied Physics A
Materials
Science & Processing

Electrical transport measurements on single-walled carbon nanotubes

J. Nygård[1,*], D.H. Cobden[1], M. Bockrath[2], P.L. McEuen[2], P.E. Lindelof[1]

[1] Ørsted Laboratory, Niels Bohr Institute, Universitetsparken 5, DK-2100 Copenhagen, Denmark
[2] Department of Physics, University of California at Berkeley and Lawrence Berkeley National Laboratory, Berkeley, CA 94720, USA

Received: 17 May 1999/Accepted 18 May 1999/Published online: 4 August 1999

Abstract. We review transport measurements on single-walled carbon nanotubes contacted by metal electrodes. At room temperature some devices show transistor action similar to that of p-channel field effect transistors, while others behave as gate-voltage independent wires. At low temperatures transport is usually dominated by Coulomb blockade. In this regime the quantum eigenstates of the finite-length tubes can be studied. At higher temperatures power law behaviour is observed for the temperature and bias dependence of the conductance. This is consistent with tunneling into a one-dimensional Luttinger liquid in a nanotube. We also discuss recent developments in contacting nanotubes which should soon allow study of their intrinsic transport properties.

PACS: 72.80.Rj; 73.23.Hk; 85.65.+h

The remarkable electrical properties of carbon nanotubes make them ideal candidates for molecular electronic devices, important both for scientific and technological applications. Not only do they provide by far the most ideal one-dimensional (1D) electron system yet discovered, but they also come with a variability of their band structure which offers the potential for constructing a wide range of electronic devices. Depending on the roll-up vector (N,M) which specifies the way the graphene sheet is wrapped to form the tube (see, e.g. [1]), they may be robustly metallic ($N = M$, 'armchair' tubes), weakly metallic ($N - M = 3p$, where p is integer) or semiconducting (all others). These band structure predictions have recently been confirmed in a very direct way by tunneling spectroscopy of individual single-walled nanotubes using low-temperature scanning tunneling microscopes [2, 3]. Furthermore, the strength and length (many μm) of nanotubes makes it relatively straightforward to attach metallic electrodes to them. Electron-beam or other types of lithography can be used to define the electrodes and if necessary align them to the tubes.

Consequently, a number of transport studies have already been performed on individual multiwalled nanotubes (MWNTs) [4–8] and on single-walled nanotubes (SWNTs) [9–16]. This paper is a review of results for SWNTs. The data presented is our own except where indicated, though in many cases is it used to illustrate features of the behaviour which have also been observed by other groups.

Some SWNT devices (see Sect. 1) are found to act as transistors [10, 16] (Sect. 2.1) at room temperature, $T \sim 300$ K. Others act as wires whose conductance is almost independent of gate voltage (Sect. 2.2) [9, 13]. So far therefore the prospects seem rosy for nanotube-based electronics. At low temperatures, more exotic behavior is seen. Much of it can be interpreted using the framework of mesoscopic physics, established mainly in the context of low-T transport measurements in microfabricated semiconductors and metals over the last two decades [17]. In most published reports so far the low-T conductance has been dominated by Coulomb blockade (Sect. 3) [9, 11–14, 18]. However, the nearly ideal 1D electronic character of nanotubes also produces less conventional phenomena. For instance, the anomalous temperature dependence [15] of nanotube devices outside the Coulomb blockade regime (Sect. 4.1) has been shown to be explicable if, as predicted [19, 20], the electrons in a metallic nanotube behave as a Luttinger liquid (Sect. 4.2). Finally, evidence is just emerging that surprisingly good metallic contacts can be achieved between normal metals and nanotubes, allowing both their use as effective electrical connections and the study of physics of transport in 1D (Sect. 5).

1 From raw material to nanotube devices

The raw material, usually grown by laser ablation [21], contains a large fraction of long, tangled, endless SWNT ropes (bundles of SWNTs). The devices we wish to realize consist of individual SWNTs or thin ropes connecting two or more metal contacts. The material is suspended and cut by ultrasounding in a solvent: dichloroethane seems most effective for cutting. Deposition, which must be immediately after ultrasounding to prevent the tubes from coagulating, is usually made on a SiO_2 substrate by wetting it with the suspension for a certain time. Tapping-mode atomic force microscope (AFM) images then reveal tube and rope segments a few μm long, interspersed with lumps of mainly graphitic material. We define our electrode patterns by electron beam lithography, using evaporated gold, sometimes with a chro-

* (E-mail: nygard@nbi.dk)

mium adhesion layer. Other metals, including platinum and aluminium, have also been used [9, 11]. The lithographic resolution is typically 50 nm, and the electrode separation between 0.1 and 1 μm.

Two approaches are possible: the electrode metal may be evaporated on top of the tubes ('metal-on-tube'); or the tubes may be deposited on top of prefabricated electrodes ('tube-on-metal'). In the former approach it is possible to align contacts to a particular rope [13], at the risk of the electron beam damaging the tubes. Techniques have been demonstrated for placing tubes or ropes in specific positions using an AFM tip [22, 23], by chemical treatment of the surface [24], or by growing them in location [25, 26], though these are still in their infancy. The easiest way to produce devices is still to create an array of contacts and then pick out cases where a randomly deposited tube or rope happens to bridge two or more contacts [9]. In our measurements we select devices whose conductance is dominated by a tube or rope of diameter at most 5 nm (as determined in the AFM), i.e., consisting of fewer than ≈ 20 tubes.

To investigate the nature of such a mesoscopic device it is crucial to have a gate electrode. For this we use a $p++$ doped metallic silicon substrate beneath the 0.3- or 1.0-μm-thick SiO_2, although a nearby surface electrode may also be effective [9]. Figure 1a shows an AFM image of a random tube-on-metal device, indicating the substrate composition. The resulting device resembles a field-effect transistor, with source, drain, and gate, whose channel is the nanotube rope.

All our measurements at $T > 1.4$ K were made with the device bathed in helium gas, whereas those at lower T were in vacuum on a dilution refrigerator. In most cases a bias voltage V and a gate voltage V_g were applied to the drain and gate electrodes, respectively, and the current out of the source was monitored with a virtual-earth current preamplifier.

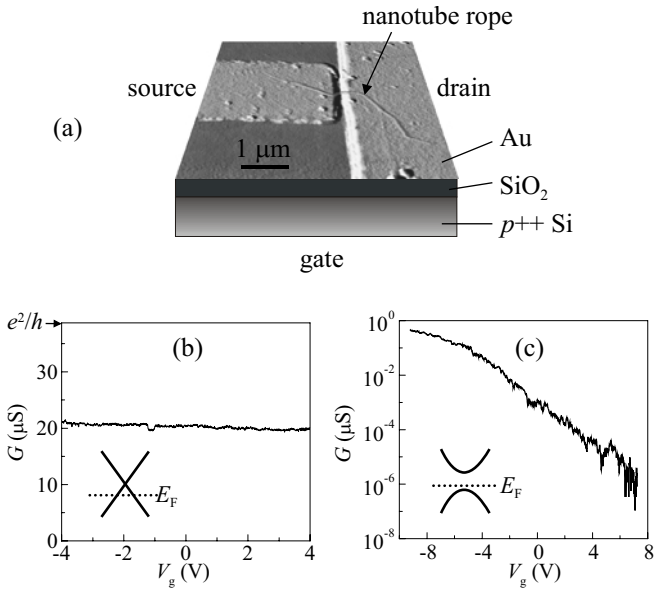

Fig. 1. a Schematic of a nanotube device. The AFM image shows a nanotube rope bridging a 200-nm gap between two gold electrodes on a SiO_2 surface. The metallically doped Si substrate is used as a back gate. **b** and **c** Conductance vs. gate voltage at room temperature for two metal-on-tube devices. *Insets:* schematic drawing of the expected dispersion $E(k)$ near the Fermi level E_F for a metallic armchair tube (**b**) and a semiconducting tube (**c**)

2 Room-temperature properties

There is a wide variation in the behavior of nominally similar devices. The lower part of Fig. 1 shows gate sweeps at room temperature for two metal-on-tube devices which exhibit dramatically different behavior. In Fig. 1b, G is virtually independent of V_g, while in Fig. 1c, G varies exponentially with V_g. Often there is instead a gradual decrease of G towards higher V_g which may be described as intermediate between these two limiting situations. We also find many cases where there is no conduction at any gate voltage, even for a source-drain bias as large as 1 V.

These variations can be attributed to several uncontrolled factors. First, electrical contacts between tubes and metal electrodes are not yet well understood. They may for instance depend on the exact atomic structure at the interface in each individual case [27], and it may be that only a few of the tubes in a rope touch the metal electrode. Second, a broad distribution of roll-up vectors is found with no special preferred type. Therefore, around two thirds of tubes are expected to be semiconducting ($N - M$ not divisible by 3) and only as few as one in twenty are the robustly metallic armchair tubes [2, 28]. Third, many sources of disorder may also be present, for instance atomic defects, tube distortions and terminations, and substrate charge. A combination of these factors makes it likely that, if a given rope conducts, its conductance is dominated by only one or a couple of the tubes within it. In interpreting the experimental results obtained thus far we have found no cause to invoke the potential complexities arising from possible effects of coupling of this dominant tube with others in the rope, most likely having random roll-up vectors. Of course, if one is able to confidently isolate an individual tube then this is not an issue.

2.1 Molecular wires

Behaviour such as that in Fig. 1b, where G_{RT} is independent of V_g can be understood if the conductance is dominated by one or more metallic tubes. Since these tubes have no gap, as indicated in the inset to Fig. 1b, in principle changing V_g has little effect on the electrons near the Fermi level E_F. In this paper we will describe such devices as 'wire-like'. We find a broad distribution of G_{RT} up to a maximum of around $3\,e^2/h$, where $e^2/h = 38.7\,\mu S$. This is not far short of the maximum theoretical conductance of a single tube of $G = 4\,e^2/h$. Here the 4 is the number of 1D modes produced by the combination of double spin and double sublattice degeneracy. In Sects. 3 and Sect. 4 we will focus on the low-T behavior of wire-like devices, which demonstrates that the conductance is usually limited by poor contacts. Only very recently have there been reports of contacts with high enough conductance to enable measurement of the intrinsic conduction properties of nanotubes, which we will return to in Sect. 5.

2.2 Molecular transistors

Characteristics of the type in Fig. 1c were first reported Tans et al. in 1998 [10]. It constitutes the realization of a molecular transistor working at room temperature. The characteristics of

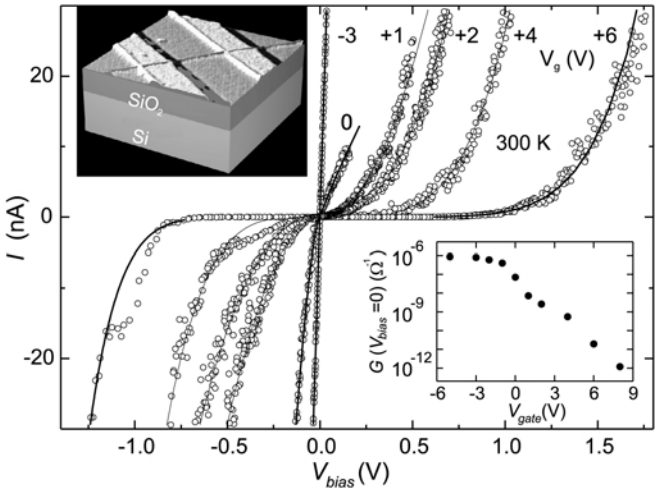

Fig. 2. The nanotube transistor ('TUBEFET'). Main: room-temperature $I-V$ traces measured in vacuum for a nanotube device at a series of gate voltages. *Left inset:* AFM image showing the nanotube lying across platinum electrodes. The gate voltage is applied to the $n+$ doped Si underneath the 300-nm-thick SiO_2 layer. *Right inset:* Small-signal conductance G vs. V_g. (Tans et al., Nature [10], courtesy of C. Dekker)

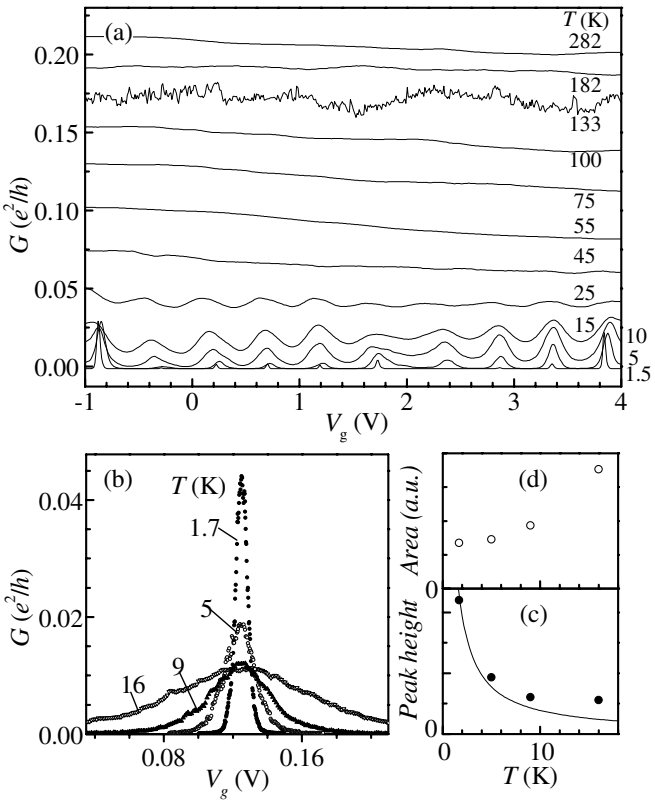

Fig. 3. a Conductance G vs. gate voltage V_g at temperatures from 282 K to 1.5 K for a metal-on-tube device. The device noise (conductance fluctuations in time) has been filtered from all traces except the one at 133 K where its amplitude is at a maximum. **b** Profile of a CB peak in another device between 16 K and 1.7 K. **c** Peak height vs. T for the peak in **b**. The *solid curve* illustrates $G \approx 1/T$. **d** Peak area vs. T

one such 'TUBEFET' are reproduced in Fig. 2 This is a tube-on-metal device, with platinum electrodes. The AFM image, in the left inset to Fig. 2 of the conducting object reveals its thickness to be only around 1 nm, consistent with it being a single tube. The right inset to Fig. 2 shows that, as in our metal-on-tube device of Fig. 1c the linear response conductance G increases by six orders of magnitude as V_g is reduced from $+6$ V to -3 V, before saturating at $\sim 1\,\mu$S at lower V_g. Also note that the $I-V$ characteristics depend strongly on V_g. For negative V_g the $I-V$ traces are linear, whereas as V_g becomes more positive they are highly nonlinear with an increasing bias threshold.

These results may be explained qualitatively if conduction occurs through a semiconducting tube, so that the device behaves as a field effect transistor [10]. The fact that G increases for negative V_g implies that the induced carriers are holes and therefore that the Fermi energy in the tube is close to the bottom of the band gap, as indicated in the inset to Fig. 1c. This is consistent with the expected transfer of electrons from a graphite-like conductor to a noble-metal contact, owing to the smaller work function of graphite [2, 10]. The maximum voltage gain obtainable from this particular transistor is ≈ 0.35. It might be increased beyond unity by reducing the oxide thickness, thus increasing the capacitance between gate and tube. The gain and performance would also be improved by increasing the carrier mobility, which in such structures appears to be much lower than that of graphite [16].

3 Low-temperature properties: Coulomb blockade and quantum levels

At liquid helium temperatures the linear-response conductance completely vanishes for transistor-like devices, but not for wire-like ones. Figure 3a shows the effect of cooling on $G-V_g$ for a wire-like metal-on-tube device with $G_{RT} \approx 8\,\mu\text{S} = 0.21e^2/h$. The average conductance drops steadily with T, and develops roughly periodic oscillations below ≈ 50 K. At 4.2 K these have become peaks isolated by regions of zero conductance. These oscillations have been shown [9, 13] to result from Coulomb blockade (CB) [18]. Their occurrence implies that the charge on the rope is quantized, which in turn implies that there exist significant tunnel resistances at the contacts, segregating part of the rope into a 'quantum dot'.

Figure 3b shows a single peak at temperatures where it is separate from its neighbours. The height of the peak, plotted in Fig. 3c approaches a $1/T$ dependence as T decreases, while the area under it, plotted in Fig. 3d approaches a constant. In the theory of CB this implies that at the lowest T the device reaches the so-called quantum limit, defined by when the single-particle level spacing ΔE exceeds $k_B T$ and transport consequently occurs via one specific quantum transition for each CB peak.

The variety of behaviour seen in different devices is illustrated by the $G-V_g$ traces in Fig. 4 taken at $T = 4.2$ K and zero magnetic field, $B = 0$. The upper two traces are from metal-on-tube devices, the lower two for tube-on-metal devices. The peak sizes and spacings show various degrees of correlation on different scales. Such complications may be attributed to there being multiple quantum dots involved in the transport. These multiple dots might be formed in parallel by several conducting tubes within a rope, or in series within a single tube which is effectively broken up into segments by disorder. To avoid or at least reduce these complications, we

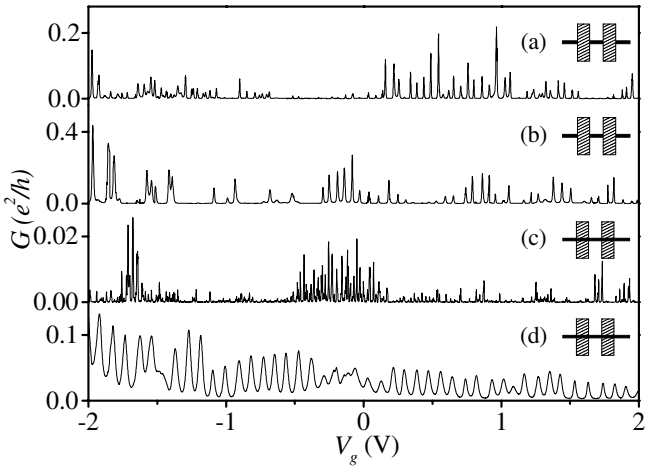

Fig. 4. $G - V_g$ for several devices at 4.2 K. As indicated by the *insets*, (a) and (b) are metal-on-tube, while (c) and (d) are tube-on-metal devices. Note that the oxide thickness is 350 nm for (a)–(c) and 1000 nm for (d)

always focus our attention on devices with wide regions of clear periodicity in V_g, indicating that they are dominated by a single quantum dot.

Figure 5a shows the device of Fig. 4a in a narrow range of V_g where the CB peaks are nearly periodic. Figure 5b shows $I - V$ traces taken at the two gate voltages marked in Fig. 5a is a grey scale plot of the differential conductance dI/dV as a function of both V_g and V. The diamond pattern seen in this 'bias spectroscopy' plot is a well understood consequence of Coulomb blockade [18]. The center of each cross, such as at $V_g = V_{g1}$, is a CB peak. At this point the ground state energies for N and $N+1$ electrons on the dot are degenerate, and there is a linear region in the $I - V$ around $V = 0$ (dashed line in Fig. 5b). In the diamonds no current flows. At some point in the diamond, such as at $V_g = V_{g2}$ (solid line in Fig. 5b), the region of zero current reaches its maximum bias V_{max}, which is a measure of the charging energy, $U = eV_{max}$, in the so-called constant-interaction model of CB. In this case we see

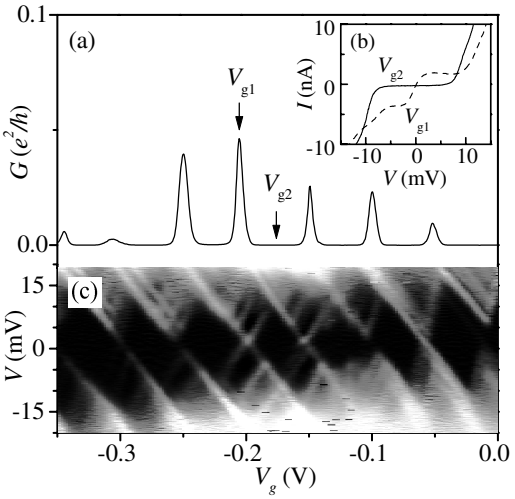

Fig. 5. a $G - V_g$ for a device at 4.2 K showing a regular series of CB peaks. **b** $I - V$ characteristics taken at the center of a peak (V_{g1}) and in between peaks (V_{g2}). **c** Grey scale (bias spectroscopy) plot of dI/dV vs. V_g and V at 4.2 K in the same range of V_g (lighter = more positive)

that $U \approx 8$ meV. Let us compare this with the very simple estimate,

$$U = \frac{e^2}{C} \approx \frac{e^2}{\epsilon_0 \epsilon_r L} \approx \frac{5\,\text{meV}}{L\,[\mu\text{m}]}. \quad (1)$$

Here we take $\epsilon_r = 4$, appropriate for SiO_2, and neglect geometrical factors which depend on the exact configuration of electrodes and are hard to estimate. To obtain $U = 8$ meV from this equation requires $L \approx 0.6\,\mu$m. Note that from U and the peak spacing $\Delta V_g \approx 50$ mV we obtain the conversion factor from gate voltage to the electrostatic dot potential ϕ_{dot} of $d\phi_{dot}/dV_g = U/e\Delta V_g = 0.16$.

The extra white lines outside the diamonds in Fig. 5c correspond to alignment of excited states with the Fermi level in either the source or the drain contact. From Fig. 5c we estimate a level spacing of $\Delta E \approx 2$ meV for this device. This is an order of magnitude greater than found typically for artificial quantum dots [18], making it exceptionally easy to resolve quantum levels in this new system. We may compare the level spacing with that expected for electrons with the appropriate dispersion confined to a 1D box of length L,

$$\Delta E = \frac{dE}{dk}\frac{\Delta k}{2} = \hbar v_F \frac{\pi}{2L} \approx \frac{1.0\,\text{meV}}{L[\mu\text{m}]}. \quad (2)$$

Here we take the Fermi velocity v_F to be that of graphite, $v_F = 8.1 \times 10^5$ m/s [29], and the factor $1/2$ accounts for the two sublattice bands, assuming their degeneracy is lifted (spin, or Kramers, degeneracy cannot be lifted at $B = 0$). To get $\Delta E \approx 2$ meV from this requires $L \approx 0.5\,\mu$m.

Thus the measured values of U and ΔE above are both consistent with charging a nanotube segment of length $L \approx 0.5\,\mu$m. This is equal to the lithographically defined contact separation for this device. In fact, we find it to be generally the case for metal-on-tube devices that U and ΔE are determined by the contact spacing: hence the similarity of the $G - V_g$ traces in Figs. 4a and 4b, which are from devices of identical geometry. This implies that the contacts define the ends of the active tube segment, that is, the evaporated metal strongly perturbs the tubes underneath it. In contrast, for tube-on-metal devices (Figs. 4c and 4d), U varies much more between devices. It often appears to correspond closely to charging the full length of the tube or rope [9], implying that the electron states are extended along the molecule lying over the contacts.

Figure 6 shows the effect of decreasing the temperature further, to 100 mK. These are measurements on another metal-on-tube device, having $U \approx 30$ meV and $\Delta E \approx 5$ meV, corresponding to the contact separation $L \approx 200$ nm. The CB peaks are now sharp spikes (Fig. 6a), whose width is limited by device noise rather than by temperature. Figure 6b is a bias spectroscopy plot of the region containing peaks labeled P, Q, R. The lines corresponding to excited state transitions are now very sharp.

A magnetic field B applied perpendicular to the tube axis is expected to modify the band structure via an Aharonov-Bohm type phase [30]. Aharonov-Bohm oscillations have indeed recently been reported in the resistance of multiwalled tubes in this geometry [4]. The diameter of SWNTs is however too small for the field to have a large effect at 12 T, where the flux linked is only $\sim \pi r^2 B \sim (1/200)h/e$ (assuming a radius $r = 7$ Å). On the other hand, with a g-factor of 2.0

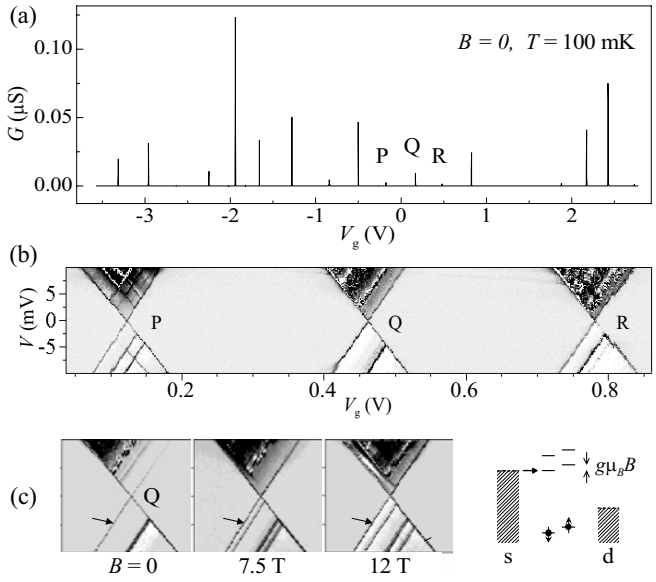

Fig. 6. **a** $G - V_{\rm g}$ for a device at 100 mK. **b** Bias spectroscopy plot for the region including peaks labeled P, Q, R in **a**. **c** Effect of magnetic field on peak Q. *Inset:* schematic interpretation of the splitting of lines in **c** as due to Zeeman splitting of single-electron levels

expected for the conduction electrons in nanotubes [31], at 12 T the Zeeman splitting $g\mu_{\rm B}B = 1.4$ meV should be easily resolved at $T = 100\,{\rm mK}(k_{\rm B}T = 8.6\,\mu{\rm eV})$.

The effect of a magnetic field on peak Q is shown in Fig. 6c Some of the lines, such as the one marked with an arrow, split proportionally to B [9, 14]. The splitting corresponds accurately to a Zeeman splitting with $g = 2.0$. This demonstrates that, in contrast with the situation in semiconductor quantum dots, thanks to the absence of orbital effects in tubes it is straightforward to study the spin of the system. For instance, the splitting of the particular line marked with an arrow indicates that the transition corresponds to adding an electron to an even number of electrons in a total-spin-zero ground state, as indicated in the sketch next to Fig. 6c [14]. So far, our own results point to an unsurprising absence of polarization of the ground state in the tube. However, more complicated magnetic-field dependences have been seen by others (in a field perpendicular to the axis) and attributed to partial ground state polarization [11].

So far only the properties of a small number of consecutive CB peaks have been studied. This is because the CB is rarely, if ever, found to be regular over a series of more than half a dozen peaks. However, the statistical properties of nanotube quantum dots, such as of the CB peak heights and spacings, should in the future provide a very useful comparison with those of 2D semiconductor dots [18]. The preditions of, for instance, quantum chaos and random matrix theory are dramatically different for these systems of different dimensionality.

4 Intermediate temperatures: new phenomena?

4.1 Power-law-like temperature dependences

Having discussed electrical properties of SWNT devices at room temperature (Sect. 2) and at liquid helium temperatures (Sect. 3), we now turn to the behavior at intermediate temperatures. For the device shown in Fig. 3 the conductance can be seen to decrease steadily on cooling. In Fig. 7 we plot the gate-voltage averaged conductance, $G_{\rm av}$, against T on a log–log scale for several wire-like devices. For both metal-on-tube devices (Fig. 7a) and tube-on-metal devices (Fig. 7b), we find that $G_{\rm av}$ always decreases monotonically as T decreases.

The behavior depends mainly on two things: first, the value of $G_{\rm RT}$; and second, whether the metal contacts are underneath or on top of the tubes. For the few devices with $G_{\rm RT} > e^2/h$, all of which are of the metal-on-tube variety, the T dependence is weak. We will discuss these further in Sect. 5. For most devices however, $G_{\rm RT} < e^2/h$, and the conductance decreases steadily from room T until it is eventually suppressed rapidly by CB at low T. The data for these devices are indicated by open symbols in Fig. 7 We do not plot the conductance at the lowest T, where CB dominates, and at higher T we multiply G by a correction factor, which varies between one and two, to compensate for the effect of classical CB [15].

We see in Fig. 7b that the T-dependences of all tube-on-metal devices look alike. From room T downwards they closely resemble a power law, $G \propto T^{\alpha}$, with $\alpha \approx 0.37$, as indicated by the dotted line. For the metal-on-tube devices in Fig. 7a the T-dependences are steeper, but are also roughly described by a power law with a larger exponent, $\alpha \approx 0.7$, indicated again by a dotted line. Note also that for the majority of these devices the conductance levels off above ~ 100 K.

Additional evidence that the low-energy physics is governed by something other than CB can be found by studying very long SWNT ropes, where the charging energy is smaller. Fig. 8 shows data from a tube-on-metal device, an AFM image of which is shown in the left inset. The rope length is $L \approx 8\,\mu$m, and the measured charging energy is accord-

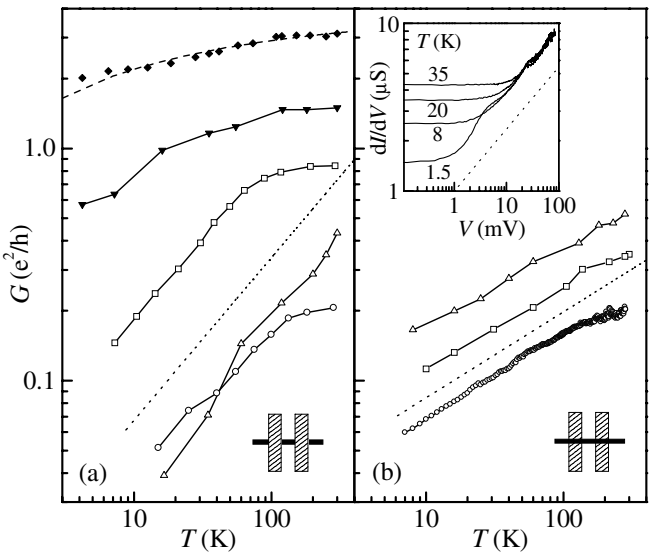

Fig. 7a,b. Conductance (averaged over $V_{\rm g}$) vs. temperature for several devices. The data plotted with *open symbols* have been corrected for Coulomb blockade, whereas the others have not. **a** Metal-on-tube devices. The *open circles* correspond to the data in Fig. 3. The *dotted line* indicates $G \propto T^{0.7}$. The *dashed line* is a fit to $G = G_0 - aT^b$ with $G_0 = 4$, giving $b = -0.22$. **b** Tube-on-metal devices. The *dotted line* here indicates $G \propto T^{0.37}$. *Inset:* ${\rm d}I/{\rm d}V$ vs. V at several temperatures for a tube-on-metal device. The *dotted line* here indicates ${\rm d}I/{\rm d}V \propto V^{0.37}$

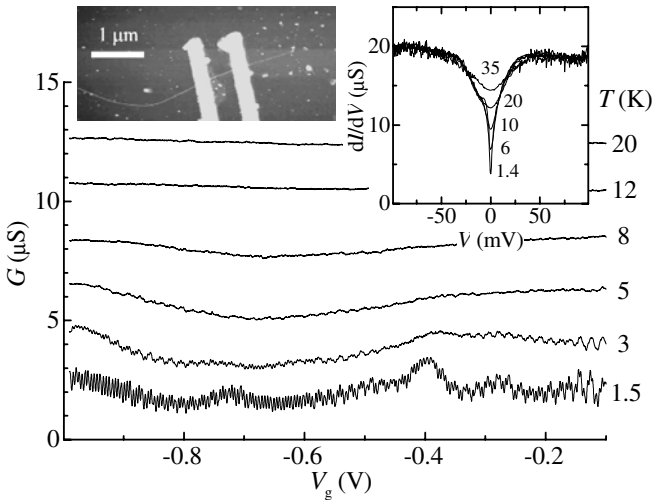

Fig. 8. $G - V_g$ for a long tube-on-metal device measured from 20 K down to 1.5 K. *Left inset:* AFM image showing the ≈ 8-μm long rope lying on top of two electrodes. The scale bar is 1 μm. *Right inset:* dI/dV vs. bias voltage V measured from 35 K to 1.4 K

ingly $U \approx 0.5$ meV. Correspondingly, in the $G - V_g$ traces, CB oscillations appear only below $T \approx 5$ K, while as usual the conductance shows a gradual increase with T at higher T. The right inset shows dI/dV vs. V at temperatures from 1.4 to 35 K. Even at 35 K, where $k_B T \gg U$ and CB therefore has no effect, a distinct anomaly around zero bias is observed. A remarkably similar zero-bias anomaly has also very recently been observed in MWNTs [5].

Since the power-law behavior is observed outside the CB regime, we must consider other possible sources for a strong T dependence of G. Thermal activation, such as might arise from transport across barriers formed in the tubes or at the contacts [12], simply bears no resemblence to a sublinear power law. Sequential transport through multiple dots can result in complex T dependences [12], but as discussed in Sect. 3 we study only devices that act as single dots. Scattering by phonons, and in particular twisting modes of the tubes [32], may explain a moderate decrease in the conductance with T at high T occasionally observed [23, 33, 34]. However it cannot explain the *increase* in G with increasing T, the gradual nature of the variation over more than an order of magnitude in T, or the observed difference between metal-on-tube and tube-on-metal devices. The cause of the T dependence must therefore be sought elsewhere.

4.2 Luttinger liquids

For a system of electrons confined to a 1D wire, interactions are predicted to lead to the formation of a so-called Luttinger liquid (LL). In a LL, the low-energy excitations of the electron system which carry current are collective modes, or waves of charge density, instead of electron-like quasiparticles [35]. The LL is characterised by a parameter g which is < 1 for repulsive Coulomb interactions. If a current is passed from a normal metal contact into an LL through a tunnel barrier, the tunneling rate is suppressed at low energies, resulting in power laws for the linear response conductance,

$$G \sim T^{\alpha} \tag{3}$$

at small biases, $eV < k_B T$, and the differential coductance,

$$dI/dV \sim V^{\alpha} \tag{4}$$

at higher biases, $eV \gg k_B T$. The exponent depends on the geometry, and is given by

$$\alpha_{\text{end}} = (g^{-1} - 1)/4 \tag{5}$$

for tunneling into the end of the LL, and

$$\alpha_{\text{bulk}} = (g^{-1} + g - 2)/8 \tag{6}$$

for tunneling into the bulk [15, 19, 20, 35].

Since metallic SWNT's are almost ideal 1D conductors, their transport properties are predicted to show the signatures of LLs [19, 20]. An estimate for the Luttinger parameter for a finite-length tube or rope is [20, 36]

$$g = (1 + 2U/\Delta E)^{-1/2}. \tag{7}$$

Notice that (1) and (2) imply that $U/\Delta E$ is independent of L. To within experimental uncertaintly we indeed find a fairly constant value of $U/\Delta E \sim 6$ [9, 13]. This gives $g \approx 0.28$, leading to $\alpha_{\text{end}} \approx 0.65$ and $\alpha_{\text{bulk}} \approx 0.24$.

Let us attempt to relate these predictions to the measurements. The observation that $G \sim T^{\alpha}$ experimentally is clearly suggestive, since tunneling between the tube and either one or both of the contacts certainly dominates the conductance of our devices at low T. We also notice that $\alpha = 0.7$ for the metal-on-tube devices is similar to α_{end}, while $\alpha = 0.37$ for the tube-on-metal devices is closer to α_{bulk}. This can be explained as follows: recall that the measurements in the CB regime (Sect. 3) implied that in the metal-on-tube case the electrons are confined to the section of tube or rope between the contacts. In this case, therefore, current-carrying electrons tunnel from the contact into the ends of this section. On the other hand, in the tube-on-metal case the electrons are only confined by the physical ends of the tube/rope. In these, therefore, electrons must tunnel from the contacts into the bulk of the electron liquid.

We may also compare the measured bias dependence with theory. The inset to Fig. 7b shows $dI/dV - V$ traces at several T for a tube-on-metal device. At high bias they converge parallel to a line (on this log–log plot) of slope $\alpha = 0.37$. This is the same exponent as for $G(T)$; exactly as expected from (4). A more detailed fit of $I(V, T)$ to a general expression is also possible [15], taking into account the partition of the voltage drop across the two different contacts.

Taken as a whole, the experimental temperature and bias dependences provide strong evidence that the electrons in metallic SWNTs form a Luttinger liquid, even at room temperature.

5 Better electrical contacts

In Sects. 3 and 4 we have discussed devices with $G_{\text{RT}} < e^2/h$ and shown that their conductance is dominated by tunneling between contacts and tubes. However, good metallic contacts to SWNTs are desirable for technological applications and also for probing their intrinsic transport properties.

Some of our metal-on-tube devices (see Fig. 7a) in fact have $G_{RT} > e^2/h$. The one in Fig. 7 with $G_{RT} \approx 3\ e^2/h$, is made from a rope no thicker than 2 nm. This suggests that high-transparency contacts exist to one or two metallic nanotubes in the rope [37]. This is supported by the fact that the device shows no CB for T as low as 1 K, together with a much weaker T dependence than the power law behavior discussed above.

Even with perfect contacts, any finite disorder within an LL is expected to completely suppress its conductance at sufficiently low T [35]. For a single impurity in a single tube, a power law suppression of G from the ideal value $G_0 = 4e^2/h$ [36] is predicted at high T. In Fig. 7 the dashed line is a fit of G_{av} to the form $G_0 - aT^b$, yielding $b = -0.22$. This value of b is rather different from the single-impurity prediction $b = (g-1)/2 \approx -0.36$ [36]. However, bearing in mind the unknown details of the disorder in the device, the qualitative agreement with a power law suppression is quite encouraging.

Recently some other groups have reported progress in achieving metallic contact to tubes without severely damaging them. Reflecting our findings for SWNTs, highly metallic contacts can be made to MWNTs simply by evaporating gold directly on top of them [4, 5]. Two-terminal conductances up to e^2/h at room T have been achieved in SWNT tube-on-metal devices by planarizing the electrodes on the SiO_2 substrate [23, 38]. Very recently conductances around e^2/h were obtained in SWNTs grown on catalyst islands on a substrate and subsequently covered by Ti/Au electrodes [26]. In a rather different approach, SWNT ropes have been laser-welded into position bridging a gap between gold electrodes formed in a transmission electron microscopy membrane [39]. In this case, apparently, sufficiently good contact can be achieved to produce proximity-induced superconductivity in the tubes when the gold electrodes are evaporated on top of a superconducting metal.

6 Conclusions and outlook

We have reviewed a selection of recent transport measurements on single-walled carbon nanotubes. A variety of phenomena are observed. At room temperature devices exhibit charactistics spanning from transistor-like behavior to metallic wires. At low-temperature Coulomb blockade usually dominates and bias spectroscopy measurements allow studies of the level structure of a nanotube quantum dot. In the intermediate temperature range, we find power-law temperature dependences which can be attributed to the existence of Luttinger liquids in the metallic nanotubes.

While the random deposition methods used so far have proven very effective for making first-generation devices, they are clearly not practical for more complicated devices or for duplicating identical devices. Every device made so far is in fact unique. To address this problem, as mentioned in Sect. 1, techniques are being developed for controlling the position and orientation of tubes on the substrate. Also, separated (unbundled) SWNTs of a fairly controlled length [40] should soon be in supply. However, the biggest challenge that lies ahead is no doubt to control the exact type of tubes built into devices. Selecting or distinguishing the roll-up vector is greatly hindered by the close structural and chemical similarity between all SWNTs with similar diameter. So far, only a high quality scanning-tunneling-microscope image can lead to reasonable certainty about the roll-up vector of a particular tube. Unfortunately, explicit knowledge of the roll-up vectors in our devices is of course highly desirable for fully investigating their electronic properties.

Nanotube electronics is a new and rapidly growing field. The situation is reminiscent of the excitement over new 2D electron systems in semiconductors two decades ago, especially with the discoveries of the quantum Hall effects. The analogous dances of interacting electrons in 1D can now be studied practically. The observation of Luttinger liquid behavior only serves to underline the remarkable nature of these fascinating molecules.

Acknowledgements. We would like to thank Leon Balents, Cees Dekker, Reinhold Egger, Karsten Flensberg and Jia Lu, for help and discussions, and Andrew G. Rinzler and Richard E. Smalley for supplying the SWNT material.

References

1. M.S. Dresselhaus, G. Dresselhaus, P.C. Eklund: *Science of Fullerenes and Carbon Nanotubes* (Academic Press, New York 1996); R. Saito, G. Dresselhaus, M.S. Dresselhaus: *Physical Properties of Carbon Nanotubes* (Imperial College Press, London 1998)
2. J.W.G. Wildöer, L.C. Venema, A.G. Rinzler, R.E. Smalley, C. Dekker: Nature **391**, 59 (1998)
3. T.W. Odom, J.-L. Huang, P. Kim, C. Lieber: Nature **391**, 62 (1998)
4. A. Bachtold, C. Strunk, J.-P. Salvetat, J.-M. Bonard, L. Forro, T. Nussbaumer, C. Schönenberger: Nature **397**, 673 (1999).
5. C. Schönenberger, A. Bachtold, C. Strunk, J.-P. Salvetat: Appl. Phys. A **69**, 283 (1999)
6. A.Yu. Kasumov, H. Bouchiat, B. Reulet, O. Stephan, I.I. Khodos, Yu.B. Gorbatov, C. Colliex: Europhys. Lett. **43**, 89 (1998)
7. L. Langer, V. Bayot, E. Grivei, J.-P. Issi, J.P. Heremans, C.H. Olk, L. Stockman, C. Van Haesendonck, Y. Bruynseraede: Phys. Rev. Lett. **76**, 479 (1996)
8. T.W. Ebbesen, H.J. Lezec, H. Hiura, J.W. Bennett, H.F. Ghaemi, T. Thio: Nature **382**, 54 (1996)
9. S. Tans, M.H. Devoret, H. Dai, A. Thess, R.E. Smalley, L.J. Geerligs, C. Dekker: Nature **386**, 474 (1997)
10. S. Tans, A.R.M. Verschueren, C. Dekker: Nature **393**, 49 (1998)
11. S. Tans, M.H. Devoret, R.J.A. Groeneveld, C. Dekker: Nature **394**, 761 (1998)
12. A. Bezryadin, A.R.M. Verschueren, S. Tans, C. Dekker: Phys. Rev. Lett. **80**, 4036 (1998)
13. M. Bockrath, D.H. Cobden, P.L. McEuen, N.G. Chopra, A. Zettl, A. Thess, R.E. Smalley: Science **275**, 1922 (1997)
14. D.H. Cobden, M. Bockrath, P.L. McEuen, A.G. Rinzler, R.E. Smalley: Phys. Rev. Lett. **81**, 681 (1998)
15. M. Bockrath, D.H. Cobden, J. Lu, A.G. Rinzler, R.E. Smalley, L. Balents, P.M. McEuen: Nature **397**, 598 (1999)
16. R. Martel, T. Schmidt, H.R. Shea, T. Hertel, Ph. Avouris: Appl. Phys. Lett. **73**, 2447 (1998)
17. C.W.J. Beenakker, H. van Houten: Solid State Physics **44**, 1 (1991); *Mesoscopic Phenomena in Solids*, ed. by B.L. Altshuler, P.A. Lee, R.A. Webb (Elsevier 1991)
18. L. Kouwenhoven, C.M. Marcus, P.L. McEuen, S. Tarucha, R.M. Westervelt, N.S. Wingreen: In *Mesoscopic Electron Transport*, ed. by L. Kouwenhoven, G. Schön, L.L. Sohn (Kluwer, Dordrecht, The Netherlands 1997)
19. R. Egger, A. Gogolin: Phys. Rev. Lett. **79**, 5082 (1997)
20. C. Kane, L. Balents, M.P.A. Fisher: Phys. Rev. Lett. **79**, 5086 (1997)
21. A. Thess, R. Lee, P. Nikolaev, H. Dai, P. Petit, J. Robert, C. Xu, Y.H. Lee, S.G. Kim, A.G. Rinzler, D.T. Colbert, G.E. Scuseria, D. Tomanek, J.E. Fischer, R.E. Smalley: Science **273**, 483 (1996)
22. Ph. Avouris: private communication

23. C. Dekker: private communication
24. J. Liu, M.J. Casavant, M. Cox, D.A. Walters, P. Boul,W. Lu, A.J. Rimberg, K.A. Smith, D.T. Colbert, R.E. Smalley: Chem. Phys. Lett. **303**, 125 (1999)
25. J. Kong, H.T. Soh, A.M. Cassell, C.F. Quate, H. Dai: Nature **395**, 878 (1998)
26. H.T. Soh, A.F. Morpurgo, J. Kong, C.M. Marcus, C.F. Quate, H. Dai: Appl. Phys. Lett. **75**, 627 (1999)
27. A. Rochefort, D.R. Salahub, Ph. Avouris: Chem. Phys. Lett. **297**, 45 (1998)
28. A. Hassanien, A. Tokumoto, Y. Kumazawa, H. Kataura, Y. Maniwa, S. Suzuki, Y. Achiba: Appl. Phys. Lett. **73**, 3839 (1998)
29. P.R. Wallace: Phys. Rev. **71**, 622 (1947)
30. H. Ajiki, T. Ando: J. Phys. Soc. Japan **62**, 1255 (1993)
31. P. Petit, E. Jouguelet, J.E. Fischer, A.G. Rinzler, R.E. Smalley: Phys. Rev. B **56**, 9275 (1997)
32. C.A. Kane, E.J. Mele: Phys. Rev. Lett. **79**, 1932 (1997)
33. J.E. Fischer, H. Dai, A. Thess, R. Lee, N.M. Hanjani, D.L. Dehaas, R.E. Smalley: Phys. Rev. B **55**, R4921 (1997)
34. C.L. Kane, E.J. Mele, R.S. Lee, J.E. Fischer, P. Petit, H. Dai, A. Thess, R.E. Smalley, A.R.M. Verschueren, S. Tans, C. Dekker: Europhys. Lett. **41**, 683 (1998)
35. M.P.A. Fischer, A. Glazman: In *Mesoscopic Electron Transport*, ed. by L. Kouwenhoven, G. Schön, L.L. Sohn (Kluwer, Dordrecht, The Netherlands 1997)
36. R. Egger, A. Gogolin: Eur. Phys. J. B **3**, 281 (1998)
37. J. Nygård, D.H. Cobden, P.E. Lindelof: unpublished
38. Z. Yao et al.: unpublished
39. A.Y. Kasumov, R. Deblock, M. Kociak, B. Reulet, H. Bouchiat, I.I. Khodos, Y.B. Gorbatov, V.T. Volkov, C. Journet, M. Burghard: Science **284**, 1508 (1999)
40. J. Liu, A. Rinzler, H. Dai, J. Hafner, R. Bradley, A. Lu, K. Shelimov, C. Huffman, F. Rodriguez-Macias, P. Boul, T. Iverson, D.T. Colbert, R.E. Smalley: Science **280**, 1253 (1998)